A Multiyear Dataset of SSM/I-Derived Global Ocean Surface Turbulent Fluxes

Shu-Hsien Chou
Laboratory for Atmospheres
NASA Goddard Space Flight Center
Greenbelt, Maryland

Chung-Lin Shie
Science Systems & Applications, Inc.
Lanham, Maryland

Robert M. Atlas
Laboratory for Atmospheres
NASA Goddard Space Flight Center
Greenbelt, Maryland

Joe Ardizzone
General Sciences Corporation
Laurel, Maryland

Eric Nelkin
Science Systems & Applications, Inc.
Lanham, Maryland

Bulletin of the American Meteorological Society
March 2001

Corresponding author: Dr. Shu-Hsien Chou, Code 912, Laboratory for Atmospheres, NASA Goddard Space Flight Center, Greenbelt, MD 20771.
E-mail: chou@agnes.gsfc.nasa.gov

ABSTRACT

A dataset including daily- and monthly-mean turbulent fluxes (momentum, latent heat, and sensible heat) and some relevant parameters over global oceans, derived from the Special Sensor Microwave/Imager (SSM/I) data, for the period July 1987-December 1994 and the1988-94 annual- and monthly-mean climatologies of the same variables is created. It has a spatial resolution of 2.0°x2.5° latitude-longitude. The retrieved surface air humidity is found to be generally accurate as compared to the collocated radiosonde observations over global oceans. The retrieved wind stress and latent heat flux show useful accuracy as verified against research quality measurements of ship and buoy in the western equatorial Pacific. The1988-94 seasonal-mean wind stress and latent heat flux show reasonable patterns related to seasonal variations of the atmospheric general circulation. The patterns of 1990-93 annual-mean turbulent fluxes and input variables are generally in good agreement with one of the best global analyzed flux datasets that based on COADS (comprehensive ocean-atmosphere data set) with corrections on wind speeds and covered the same period. The retrieved wind speed is generally within ± 1 m s^{-1} of the COADS-based, but is stronger by ~1-2 m s^{-1} in the northern extratropical oceans. The discrepancy is suggested to be mainly due to higher COADS-modified wind speeds resulting from underestimation of anemometer heights. Compared to the COADS-based, the retrieved latent heat flux and sea-air humidity difference are generally larger with significant differences in the trade wind zones and the ocean south of 40°S (up to~40-60 W m^{-2} and ~ 1-1.5 g kg^{-1}). The discrepancy is believed to be mainly caused by higher COADS-based surface air humidity arising from the overestimation of dew point temperatures and from the extrapolation of observed high humidity southward into data-void regions south of 40°S. The retrieved sensible heat flux is generally within ± 5 W m^{-2} of UWM/COADS, except for some areas in the extratropical oceans, where the differences in wind speed have large impact on the difference in sensible heat flux. The dataset of SSM/I-derived turbulent fluxes is useful for climate studies, forcing of ocean models, and validation of coupled ocean-atmosphere global models.

1. Introduction

The Special Sensor Microwave/Imager (SSM/I) on board a series of the Defense Meteorological Satellite Program (DMSP) spacecraft has provided near-global coverage with improved coverage, spatial resolution, and accuracy over prior passive microwave instruments. A number of techniques have been developed to retrieve the turbulent fluxes from the SSM/I measurements (e. g., Chou et al. 1995, 1997; Clayson and Curry 1996; Curry et al. 1999; Schluessel et al. 1995; Schulz et al. 1993, 1997). This is because the global air-sea turbulent fluxes are required for driving ocean models and validating coupled ocean-atmosphere global models.

Curry et al. (1999) have produced a 50km-resolution dataset of air-sea fluxes from SSM/I data for the Coupled Ocean-Atmosphere Response Experiment (COARE) intensive observing period (IOP), from November 1992 to February 1993, in the intensive flux array (a small area in the western Pacific warm pool). Schulz and Jost (2000) have produced a global dataset of latent and sensible heat fluxes from SSM/I data for the period July 1987 to present, which is called the **H**amburg **O**cean **A**tmosphere **P**arameters and Fluxes from **S**atellite Data (HOAPS). Based on Chou et al. (1997), we have produced a Version 1 of **G**oddard **S**atellite-Based **S**urface **T**urbulent **F**luxes (GSSTF) dataset from the SSM/I data and other data. It provides daily- and monthly-mean surface turbulent fluxes and some relevant parameters over global oceans for individual DMSP F8, F10, and F11 satellites covering the period July 1987-December 1994. It also provides 1988-94 annual- and monthly-mean climatologies of the same variables, using only F8 and F11 satellite data. It has a spatial resolution of 2.0°x2.5° latitude-longitude and is available from the Distributed Active Archive Center (DAAC) of the NASA/Goddard Space Flight Center (GSFC) (http://daac.gsfc.nasa.gov/CAMPAIGN_DOCS/hydrology/hd_main.html). These three flux datasets and some other datasets will participate in the SEAFLUX intercomparison project (http://paos.colorado.edu/~curryja/ocean/home.html).

The project of comprehensive ocean-atmosphere data set (COADS) has collected the most complete surface marine observations since 1854, mainly from merchant ships (Woodruff et al.

1987; Woodruff et al. 1993). There are several air-sea flux datasets based on COADS with adjustments in data or roughness lengths for flux computations (e. g., Oberhuber 1988; da Silva et al. 1994; Josey et al. 1999). Ship-based wind speeds are mostly estimated from sea states (referred to as visual winds) using the World Meteorological Organization (WMO) 1100 Beaufort scale. It has generally been recognized that this scale underestimates wind speeds at low to moderate winds ($< \sim 19$ m s^{-1}) but overestimate wind speeds at high winds (Kent and Taylor 1997 and references within). In addition, the global distribution of ship reports is spatially inhomogeneous with a relatively large number of observations in midlatitudes of North Pacific and North Atlantic, but very few in the Southern Hemisphere (da Silva et al. 1994; Woodruff et al. 1993; Josey et al. 1999). Da Silva et al. (1994) produced 1° x 1° latitude-longitude global monthly mean air-sea fluxes for the period 1945-93 using a successive correction method (filling data gaps), based on COADS with correction on wind speeds. Josey et al. (1999) have corrected more input variables and used a similar successive correction method to generate global flux fields. However, their 1980-93 flux climatologies are generally not very different from that (1945-89) of da Silva et al. (1994).

The satellite-based flux fields are subject to retrieval errors. On the other hand, the COADS-based global analyzed flux fields may have regional biases due to errors of measurements, spatial and temporal samplings, and objective analyses (Isemer and Hasse 1987; Kent et al. 1993; da Silva et al. 1994; Kent et al. 2000). As there is no "ground truth" of global flux fields and we can not get enough in situ quality measurements over the vast oceans, it is important to conduct intercomparison studies between these two fields and available high quality in situ measurements. It can identify the strengths and weaknesses of the retrievals. It can also assess the quality of COADS-based flux fields, especially over the data-void regions of the Southern Hemisphere. To correctly evaluate the differences between various datasets, the same time periods have to be used. Thus we compare the retrieved 1990-93 annual-mean fluxes and input variables with the1990-93 results (referred to as UWM/COADS in this paper) of da Silva et al. (1994), which is recognized to be one of the best global analyzed flux datasets derived from COADS.

The purpose of this paper is to present a most updated assessment of the GSSTF 1.0 dataset. It will be useful to the future SEAFLUX intercomparison studies and researchers interested in our data. Section 2 describes the data sources used in this study. Section 3 briefly describes the methodology and validation for the retrieval of surface air humidity. To test the validity of the humidity-retrieval technique, surface air humidity retrieved from the F8 SSM/I during February and August 1988 and from the F10 and F11 SSM/Is during 1993 are compared with those collocated radiosonde observations over global oceans. Section 4 briefly describes the methodology and validation for the retrieval of turbulent fluxes. To assess the retrieval accuracy, daily turbulent fluxes retrieved from the F10 and F11 SSM/Is are compared with those derived from measurements of the RV Moana Wave during three separate cruises in the COARE IOP and the IMET buoy during the entire COARE IOP. The F10 satellite platform was misplaced in orbit, and the orbit drifted during the time of operation. To see the effect, the global distributions of 1992-94 annual mean turbulent fluxes and input variables are compared between F10 and F11 satellites in section 5. This provides some justification about why F10 measurements are not included in the climatologies of GSSTF 1.0 dataset. Section 6 presents the global distributions of 1988-94 seasonal-mean wind stresses and latent heat fluxes, derived from monthly climatologies of the GSSTF 1.0 dataset. To assess regional biases, the global distributions of 1990-93 annual-mean fluxes and input variables are compared between SSM/I and UWM/COADS in section 7. Concluding remarks are given in section 8.

2. Data sources

The datasets used to derive surface air humidity and turbulent fluxes are: 1) the SSM/I total precipitable water (total column water vapor amount) and 10-m wind speeds of Wentz (1994), 2) the precipitable water in the lowest 500-m bottom-layer, 3) the 0Z and 12Z analyses of SST–T_{2m} (2-m temperatures) and sea-level pressures of the European Centre for Medium-Range Weather Forecasts (ECMWF), 4) the weekly-mean sea surface temperatures (SST) of the National Centers for Environmental Prediction (NCEP), and 5) the SSM/I 10-m wind directions of Atlas (1996). Using the method of Schulz et al. (1993), we estimate the bottom-layer precipitable water from the

brightness temperatures derived from the SSM/I antenna temperatures of Wentz (1993). Daily mean SSTs for computing latent heat fluxes are interpolated from the weekly mean values of NCEP (Reynolds and Smith 1994).

The SSM/I is a passive microwave radiometer, which senses the earth atmosphere system at four frequencies of 19.35, 22.235, 37.0 and 85.5 GHz. It has both horizontal and vertical polarization except for the 22 GHz water vapor channel that has only the vertical polarization measurement. Wentz (1994) developed his algorithm to retrieve simultaneously the 10-m wind speed, total precipitable water, columnar cloud water, and rain rate. These four geophysical parameters were derived by matching all the brightness temperatures of the five low frequency SSM/I channels to those computed using a radiative transfer model of the atmosphere and ocean. Analyzing the retrieval error budget he found that, for a 50-km resolution, the root-mean-square (rms) accuracy was 1.0 m s^{-1} for the SSM/I wind speed, and 1.0 kg m^{-2} for the SSM/I total precipitable water. In this study, the SSM/I data used for the collocation validation of surface air humidity and turbulent fluxes are from the F8, F10, and F11 satellites. The 1990-93 annual-mean (1988-94 seasonal-mean) turbulent fluxes and input variables are derived from the F8 and F11 SSM/Is, which have slightly better data quality than the F10 SSM/I (see sections 3b and 5).

To validate the estimated surface air humidity, twice-daily radiosonde observations at 30 stations over the global oceans (Table 1) for February and August 1988 and for 1993 are used to match the SSM/I retrievals. To validate the retrieved daily turbulent fluxes, the Moana Wave flux data (1.7°S, 156°E), and the latest version of the 7.5-min mean surface fluxes at the IMET buoy (1.75°S, 156°E) are used. The former were obtained from the COARE Surface Flux Summary - Release #2 (C. Fairall, private communication, 1994), while the latter were computed by Weller and Anderson (1996). To assess regional biases, the 1990-1993 annual-mean turbulent fluxes and input variables of da Silva et al. (1994) are used.

3. Methodology and validation for retrieval of surface air humidity

a. Methodology for retrieving surface air humidity

Chou et al. (1995) developed a technique to retrieve surface air humidity from the SSM/I total precipitable water and lowest 500-m bottom-layer precipitable water (W_B). In this paper, the retrieved surface air humidity is referred to as the specific humidity at the 10-m level (Q_{10m}) as it is so used in the flux computation. The coefficients of Q_{10m} retrieval equation (see Table 1 of Chou et al. 1997) were determined from the vertical profiles of the mean and first two empirical orthogonal functions (EOFs) of a sample population of humidity soundings of a given climatic regime. To retrieve Q_{10m} over global oceans, six sample populations and EOFs corresponding to six climate regimes were generated from a total of 23177 FGGE IIb humidity soundings observed at 64 stations over global oceans during December 1978-November 1979 (Chou et al. 1995). The soundings at each station were grouped into a cold-season (November to April for the Northern Hemisphere and May to October for the Southern Hemisphere) and a warm-season. These 128 (2x64) semiannual subsets were further grouped into six sample populations, according to the semiannual-mean total precipitable water. The ranges of semiannual-mean total precipitable water of the six sample populations were set to be 0-10, 10-20, 20-30, 30-40, 40-50, and >50 kg m^{-2}. The locations and mean total precipitable water of the subsets of the sample populations are highly related to the pattern and seasonal variation of the SST (see Figs. 1 and 2 of Chou et al. 1995). These six sample populations were thus considered as representing different climatic regimes for retrieving the Q_{10m}. The Q_{10m} was assumed to be a weighted mean of three quantities derived from the humidity retrieval equations of three adjacent sample populations (or climatic regimes), which were selected by the SSM/I-retrieved total precipitable water.

Chou et al. (1995) found that the SSM/I-retrieved Q_{10m} agreed reasonably well with those of the radiosonde observations, COADS (Woodruff et al. 1987), and climatology estimated from ship measurements (Esbensen and Kushnir 1981). However, the derived Q_{10m} in the northern extratropical oceans had a negative bias in the winter but a positive bias in the summer, as compared to COADS. Chou et al. (1977) made two modifications to the original EOF method to reduce the humidity biases. The negative humidity bias over the wintertime extratropical oceans (W_B< 3 kg m^{-2}) was mainly due to underestimation of the SSM/I-retrieved W_B. Thus, they set the lower limits of

Q_{10m} to be that derived from the total precipitable water (more accurate than SSM/I W_B) in these dry regions. On the other hand, the saturation specific humidity at daily SSTs was set to be the upper limits for the Q_{10m} over the global oceans. This reduces the positive humidity bias over the summertime extratropical oceans. In the summer, when the warmer continental (or maritime) air moves over a colder ocean surface, fog or stratus may form with the surface air reaching saturation at a temperature near the underlying cold SST. Under this situation, the original method tends to overestimate Q_{10m}. Chou et al. (1997) found that the global distributions and seasonal variability of the retrieved monthly surface air humidity (and latent heat fluxes) were more realistic than those of Chou et al. (1995), as a result of these two modifications.

b. Collocation validation for retrieved surface air humidity

To validate the retrieved Q_{10m}, radiosonde observations at 30 stations over the global oceans (Table 1) are compared with the retrievals within 100 km and 1.5 h of SSM/I measurements. Within 100 km and 1.5 h of satellite measurements, a single radiosonde observation can match many SSM/I cells (with a mean of ~50 for total precipitable water and ~30 for W_B). As these collocated SSM/I cells may not be independent samples, they are averaged and considered as a single sample for the collocation validation. Note that this approach is different from that of Schulz et al. (1997), who considered all the collocated SSM/I cells (with a smaller window) as independent samples for computing the retrieval errors. As the rms error decreases with increasing sample size, which depends on the collocation window, the retrieval accuracy presented by different studies should be compared with caution. Table 2 compares the retrieved Q_{10m} with those of radiosonde observations matched within 100 km and 1.5 h over global oceans and various regions. Comparisons are carried out for three periods: February and August 1988, February and August 1993, and the entire annual cycle of 1993. Most radiosondes are launched at 0 and 1200 UTC. The ascending equatorial crossing times are 0612, 1942, and 1702 LT for the F8, F10 and F11 satellites, respectively. The collocated data pairs for global oceans are 342 (F8) for February and August 1988, 462 (288 for F10 and 174 for F11) for February and August 1993, and 2054 (1205 for F10 and 849 for F11) for 1993.

As can be seen from Table 2, the humidity retrieval is generally accurate over global oceans for the three periods tested during 1988 and 1993. For a 25-km spatial resolution, the Q_{10m} retrieved from the F8 and F11 SSM/Is has small biases of 0.03-0.25 g kg^{-1}, rms differences of 1.55-1.62 g kg^{-1}, and a correlation coefficient of 0.97, as compared to the radiosonde observations over global oceans. The Q_{10m} retrieved from the F10 SSM/I over global oceans reduces the accuracy by 0.2-0.3 g kg^{-1} and SSM/I-radiosonde correlation by 0.03-0.04, as compared to the other two SSM/Is. The Global and regional validations show that the accuracy of Q_{10m} derived from the F8 and F11 SSM/Is is comparable and is slightly better than that derived from the F10 SSM/I.

4. Methodology and validation for retrieval of air-sea turbulent fluxes

a. Methodology for retrieving air-sea turbulent fluxes

Turbulent fluxes are derived using the best one of four stability-dependent aerodynamic bulk schemes tested against aircraft covariance fluxes measured during cold air outbreaks off the middle North Atlantic coast of the United States (Chou 1993). This scheme is similar to Fairall et al. (1996) but without a gustiness and skin SST parameterization. The former was found to have insignificant impact on the SSM/I turbulent fluxes (Chou et al. 1997). In addition, the bulk temperature instead of skin SST is used for the computation of latent and sensible heat fluxes. The von Karmen constants for the non-dimensional profiles of wind, temperature, and moisture are equal to 0.4, 0.36, and 0.45, respectively. This causes the transfer coefficient to increase 12.5% for latent heat flux but to decrease 10% for sensible heat flux, as compared to a uniform von Karmen constant of 0.4. Using the surface-layer similarity theory, the turbulent fluxes are derived from the surface-layer scaling parameters by iteratively solving the diabatic profiles of wind, temperature, and moisture. The bulk transfer coefficients are stability dependent and are functions of wind speed, and sea-air temperature and humidity differences. This scheme will be compared with other bulk schemes in the SEAFLUX intercomparison project.

Input parameters are daily-mean values of SST, saturation specific humidity at the sea surface (Q_S), wind speed and specific humidity 10 m above the surface, and air temperature 2 m above the

surface (T_{2m}). It is noted that the reference height in the bulk scheme is set to 10 m for wind speed and humidity but is set to 2 m for temperature for correctly calculating their gradients and stability (Chou et al. 1997). The SSM/I 10-m wind speeds of Wentz (1994) are used. Wind stress directions are taken from the surface wind directions of Atlas et al. (1996), which used the 10-m wind speeds of Wentz (1994) for input to a variational analysis. The retrieval of Q_{10m} is briefly discussed in the previous section. The Q_S is determined from the daily mean SST, which is interpolated from the NCEP weekly mean SSTs (Reynolds and Smith 1994). To use an aerodynamic bulk scheme to derive surface sensible heat fluxes, the measurements of air temperatures in the atmospheric surface layer (about 50-100 m) are required. However, they are not currently available from satellite measurements. Thus, the SST–T_{2m} used for computing the sensible heat flux is taken from the averages of 0Z and 12Z analyses of the ECMWF. Sea-air temperature difference is generally very small over the open ocean, except for the western Pacific warm pool and midlatitudes in the winter. Small errors in the SSTs and air temperatures could induce a relatively large error in the sea-air temperature difference if the errors are uncorrelated. The ECMWF analysis of 2-m temperatures is thermodynamically constrained to the SST.

The latent and sensible heat fluxes depend on the skin SST. The skin SST is usually 0.2-0.3°C cooler than bulk temperature with the difference depending on surface net heat flux and wind induced oceanic mixing (Webster et al. 1996; Wick et al. 1996 and references within). The global distribution of true skin SST for the period interested is not currently available, as its determination is very challenging and is still underdeveloped by various scientists (see the SEAFLUX intercomparison project). In addition, the daily-mean value of the bulk-skin SST difference is usually insignificant due to day-night cancellation. It may even be smaller than the error of the estimated skin SST, which arises from the uncertainty in the surface heat budgets, wind speeds, and skin SST parameterization. Thus we use the bulk temperatures of global oceans analyzed by the NCEP and ECMWF to compute heat fluxes in our GSSTF 1.0 dataset and this paper.

b. Collocation validation for retrieved air-sea turbulent fluxes

Chou et al. (1997, 2000) have validated the daily air-sea turbulent fluxes, derived from the F10 and F11 SSM/Is, with those computed from measurements of the RV Moana Wave and IMET buoy during the COARE IOP (November 1992 to February 1993). These results are summarized in Table 3. For the latent heat fluxes (wind stresses) of the RV Moana Wave, Chou et al. (1997) used 59% (77%) of covariance fluxes and 41% (23%) of the bulk fluxes computed by Fairall et al. (1996). They derived daily mean sensible heat fluxes at the RV Moana Wave from the 50-min bulk fluxes computed by Fairall et al. (1996), as small sensible heat fluxes estimated using the eddy correlation method might be sensitive to the measurement errors. Retrieved daily fluxes of the nearest grid box (2.0°x2.5° latitude-longitude) centered at (2°S, 155°E), were used for the comparison with the Moana Wave observations (1.7°S, 156°E). Chou et al. (2000) derived 120 days of daily mean turbulent fluxes at the IMET buoy from the latest version of the 7.5-min mean surface fluxes computed by Weller and Anderson (1996) using the bulk scheme of Fairall et al. (1996). The retrieved daily fluxes, interpolated to a 1.0°x1.0° latitude-longitude region centered at (1.5°S, 156°E), were used for the comparison with the IMET observations (1.75°S, 156°E).

Table 3 shows that the retrieval accuracy of turbulent fluxes is comparable when validating with both the RV Moana Wave and IMET buoy. Compared with the RV Moana Wave (IMET buoy), the retrieved daily wind stresses have a bias of 0.0061 (-0.0018) N m^{-2}, an rms difference of 0.0187 (0.0211) N m^{-2}, and a correlation coefficient of 0.86 (0.78). The retrieved daily latent heat fluxes (LHF) have a bias of 6.2 (-2.4) W m^{-2}, an rms difference of 29.0 (29.2) W m^{-2}, and a correlation coefficient of 0.83 (0.71). On the other hand, the retrieved daily sensible heat fluxes (SHF) are not in good agreement with those of the Moana Wave and IMET buoy. The poor quality of the retrievals is likely a result of comparing a small SHF with a large variability. Chou et al. (2000) found that the retrieval significantly underestimated peak values of SHF during episodic events of strong westerly wind bursts and squalls and suggested that to be mainly due to event-related rainfall effect. Note that the spatial variability of the turbulent fluxes may contribute to the estimated retrieval errors. The fluxes at the Moana Wave and IMET buoy are computed from the point measurements, while those of the retrievals are computed from area-mean measurements. These

results suggest that, with the assumption that daily errors are independent, the rms differences are 0.0042-0.0069 N m^{-2} for the retrieved monthly wind stress, 5.8-8.1 W m^{-2} for the retrieved monthly LHF, and 1.0-2.8 W m^{-2} for the retrieved monthly SHF.

5. Comparison of fluxes between F10 and F11 satellites

The F10 satellite platform was misplaced in orbit, and the orbit drifted during the time of operation. For the period 1988 to 1994, F10 and F11 satellite measurements are overlapped for the period 1992-94. The comparison of retrieval differences between F10 and F11 during these three years provides an opportunity to see the effect of the orbital drift of the F10 satellite. Figure 1 shows F10-F11 differences of retrieved 10-m wind speed, 10-m specific humidity, and LHF for 1992-94. It can be seen from Fig. 1a that the 10-m wind speed is slightly smaller for F10 than for F11. The difference is less than 0.4 m s^{-1}, except in the areas of tropical convergence and the western North Pacific and North Atlantic, with a mean difference of 0.22 m s^{-1} over the global oceans. This result is consistent with that found by Wentz's group. They found averaged SSM/I-buoy differences of 10-m wind speed of -0.406 and 0.103 m s^{-1} for F10 and F11, respectively (http://www.ssmi.com). Their result and Fig.1a suggest that wind speed and stress have slightly better retrieval accuracy for F11 than for F10. The retrieval differences of wind speed and surface air humidity between the two satellites may be caused by the orbital drift of the F10 satellite.

Figure 1b shows that the Q_{10m} is systematically smaller for F10 than for F11, with a significant difference of 0.8-1.0 g kg^{-1} in the subtropics and the southern trade wind regions. Differences of 0.5-0.6 g kg^{-1} are found in the tropical convergence areas, with the minimum difference in the areas towards high latitudes. The difference in the Q_{10m} results in a significant LHF difference of 20-30 W m^{-2} in the subtropics and the southern trade wind regions, but decreasing toward tropical convergence zones and high latitudes (Fig. 1c). In the equatorial Indian ocean and western Pacific warm pool, the LHF of F10 is larger than that of F11 by a very small value of < 5 W m^{-2}, as the effect due to differences in wind speeds compensate that of Q_{10m}. Note that averaged over the COARE IOP (November 1992-February 1993) at the grid point (2°S, 155°E) most close to the

IMET buoy, the F10-F11 differences of LHF (0.5 W m^{-2}) and SHF (-0.6 W m^{-2}) are very small. However, the F11-derived wind stress is 0.0126 N m^{-2} larger than that of F10 and is closer to the IMET measurement. In addition, the F10-F11 differences of Q_{10m} shown in Fig.1b are consistent with the differences of Q_{10m} retrieval biases for regional validations shown in Table 2. The results again suggest a better retrieval accuracy of Q_{10m} for F11 than for F10. Averaged over global oceans for 1992-94, the10-m wind speed is smaller by 0.22 m s^{-1}, the Q_{10m} is smaller by 0.59 g kg^{-1}, but the latent heat flux is larger by 14.4 W m^{-2} for F10 than for F11. Because the regional difference of LHF between the two satellites is significant and because the retrieval accuracy is slightly better for F11 than for F10, we only use F8 and F11 SSM/I data (excluding F10 data) to compute annual- and monthly-mean climatologies in our GSSTF 1.0 dataset.

6. 1988-94 seasonal-mean wind stresses and latent heat fluxes

In this section, we present the seasonal variations of the most important fluxes of momentum and latent heat along with their relevant parameters for the 1988-94 climatologies. Four seasons of winter (December, January, and February), spring (March, April, and May), summer (June, July, and August), and fall (September, October, and November) are used for the discussion. Figure 2 shows 1988-94 seasonal-mean wind stresses, derived from F8 (1988-91) and F11 (1992-94) SSM/Is, respectively. The maximum wind stresses and speeds (not shown) are generally found in the trade wind zones, the tropical Indian ocean (associated with the southwest summer Monsoon circulation), the wintertime extratropical North Pacific and North Atlantic oceans (associated with synoptic activities), and the extratropics of the Southern Hemisphere. Wind stresses and speeds of the trade wind zones are larger in the Northern Hemisphere than in the Southern Hemisphere during the winter and spring, and vise versa during the other two seasons, as a result of seasonal variations of the Hadley circulation. The minimum wind stresses and speeds are generally found in the tropical Indian ocean and South Pacific convergence zone (SPCZ) during the winter and spring, near Indochina during the summer and fall, the intertropical convergence zones (ITCZ) in the eastern equatorial Pacific and Atlantic Oceans, and subtropical highs. The retrieved wind stress and wind fields clearly show the seasonal variation of the atmospheric general circulation and are

consistent with those of Atlas et al. (1996), Esbensen et al. (1993), Chou et al. (1995), and Hellerman and Rosenstein (1983).

Figure 3 shows 1988-94 seasonal-mean LHF, derived from F8 (1988-91) and F11 (1992-94) SSM/Is, respectively. The seasonal variability of LHF follows essentially that of sea-air humidity difference, Q_S-Q_{10m}, (not shown). Both variables are larger in the winter than in the summer hemisphere. The maximum LHF (160-240 W m^{-2}) is generally found in the trade wind zones of both hemispheres, where the Q_S-Q_{10m} is large (5-7 g kg^{-1}) and winds are strong (7-10 m s^{-1}). In the trade wind zones, the largest values of wind speed, Q_S-Q_{10m}, and LHF are in the winter hemisphere due to the strongest wintertime Hadley circulation (see Figs 2-3). In addition, the maximum LHF (~240-280 W m^{-2}) is found in the Kuroshio Current and Gulf Stream areas (Fig. 4a). Strong winds and large Q_S-Q_{10m} prevail in these regions during the winters (not shown), due to cold air outbreaks over warm oceans (e.g., Agee and Howley 1977; Chou and Ferguson 1991; Chou 1993). The LHF and Q_S-Q_{10m} decrease poleward with decreasing SST, with the minima in high latitudes of the summer hemisphere. The minima of LHF and Q_S-Q_{10m}, associated with weak winds, are also found in the eastern equatorial Pacific and Atlantic for all seasons related to the up-welling induced cold SST. The large-scale patterns and seasonal variations of LHF and Q_S-Q_{10m} for the winter and summer are consistent with those of Chou et al. (1997).

7. Comparison with 1990-93 UWM/COADS

In this section we compare1990-93 annual-mean turbulent fluxes and input variables, derived from F8 (1990-91) and F11 (1992-93) SSM/I data, with those of UWM/COADS. Da Silva et al. (1994) have produced a dataset of 1.0°x1.0° latitude-longitude global fields of monthly-mean turbulent fluxes for the period 1945-93, which is one of the most current and best flux datasets derived from ship reports. To accurately evaluate the differences between these two datasets, the same time period of 1990-93 is used. Although both datasets overlap six years from 1988 to 1993, the comparison using these six-year data is not expected to affect our conclusion. For the comparisons, the results of UWM/COADS are interpolated to the same 2.0°x2.5° latitude-longitude

global grid as that of the SSM/I. In addition, the 20-m reference height (used in UWM/COADS) is used. The wind speeds (U_{20m}), specific humidity (Q_{20m}), and temperature (T_{20m}) of SSM/I at this level are derived from the aerodynamic bulk scheme using the retrieved fluxes.

a. Comparison of SST, surface air humidity and temperature

The patterns of 1990-93 annual-mean SST, 20-m specific humidity, and 20-m temperature (not shown) are in good agreement between SSM/I and UWM/COADS (or COADS). The differences of 1990-93 annual-mean SST, Q_{20m}, and T_{20m} between the two datasets are shown in Fig. 4. The SST difference between NCEP and COADS is generally negligibly small (Fig. 4a), while the T_{20m} is slightly cooler for ECMWF than for COADS with the maximum difference of 0.5-1°C in the extratropics (Fig. 4c). On the other hand, Fig. 4b shows that the SSM/I Q_{20m} is significantly drier than COADS (except for the equatorial Indian Ocean, western Pacific warm pool and ITCZs), with the maximum difference of 1-2 g kg^{-1} in the trade wind zones and southern oceans (south of 40°S). The maximum Q_{20m} difference in the trade wind regions of the eastern South Pacific and South Atlantic is due to the lack of dry tongues for COADS.

The humidity difference in the southern ocean shown in Fig. 4b is likely due to the objective analysis of UWM/COADS. Da Silva et al. (1994) filled the missing data using a successive correction method with the radii of influence of 1541, 1211, 881, and 771 km. Data within different radii of influence were weighted by distance and averaged in successive passes of the smoothing process. Since data are scarce in the oceans south of 40°S, high Q_{20m} observed further northward are extrapolated southward (Kent et al. 2000). This can cause UWM/COADS to have high Q_{20m} and large differences with SSM/I south of 40°S. For the three stations in the southern extratropical Pacific Ocean (52.5°S,169°E; 54.5°S,159°E) and southern extratropical Indian Ocean (38°S,77.5°E), Table 2 shows that the F11-retrieved Q_{10m} has negligibly small biases of -0.07, -0.11, and -0.13 g kg^{-1}, respectively, as compared to radiosonde observations. However, Fig. 4b shows that the Q_{20m} of UWM/COADS at these stations (see Table 1) is higher than that of SSM/I by 0.96, 1.04, and 0.75 g kg^{-1}, respectively.

Five buoys were deployed between 18° and 33°N in the eastern North Atlantic during the Subduction Experiment from June 1991 to June 1993 (Moyer and Weller 1997). Table 4 compares monthly-mean 20-m specific humidity and wind speeds of SSM/I and UWM/COADS with those derived from buoy measurements for the periods of reliable buoy records (Moyer and Weller 1997). The results for the buoys are computed from point measurements, while those of SSM/I and UWM/COADS are computed from the averages over an area of 2.0°x2.5° latitude-longitude (with the centers nearest but ~50-100 km west of the buoy locations). As the surface air humidity and wind speed increase westward in the experimental area, the spatial mismatch may cause positive biases for the SSM/I and UWM/COADS as compared to buoy measurements in Table 4. Table 4 show that the SSM/I and COADS Q_{20m} generally have comparable biases as compared to buoy measurements, except for the SW buoy of the trade wind region. Compared to the measurements at the SW buoy, the Q_{20m} has a small bias of 0.5 g kg^{-1} for SSM/I but has a relatively large positive bias of 1.2 g kg^{-1} for COADS. This result suggests the humidity overestimation of UWM/COADS to be primarily responsible for the Q_{20m} difference in the trade wind regions shown in Fig. 4b. The northeast buoy was the only one to remain operational throughout the experiment and provided the most reliable data, while the measurements at other four were less complete. Thus the measurements at the NE buoy are used to show the fidelity of the monthly variability of the SSM/I and UWM/COADS Q_{20m} during the two years of experiment in Fig. 5. It can be seen from Fig. 5 that the monthly-mean Q_{20m} for both datasets follows closely that of the NE buoy, except for slightly positive biases.

For the stations of Caribbean sea (10°N-20°N, 85°W-55°W) and equatorial Indian Ocean (15°S-15°N, 50°E-100°E), Table 2 shows that the F11-retrieved Q_{10m} has small positive biases of 0.15 and 0.51 g kg^{-1}, respectively, as compared to radiosonde observations. However, Fig. 4b shows that the Q_{20m} of UWM/COADS at the stations of these two regions (see Table 1) is higher than that of SSM/I by 0.95 and 0.29 g kg^{-1}, respectively. This result is consistent with some previous findings that ships overestimated dew point temperatures (by ~0.5°C), resulting in a higher value of surface air humidity for COADS (Isemer and Hasse 1987; Kent et al. 1993; da Silva et al.

1994; Josey et al. 1999). Chou et al. (1997) also found that the radiosonde observed Q_{10m} was closer to SSM/I than COADS. In addition, they found a 0.5°C decrease in dew point temperature for the COADS within 60°S-60°N (excluding data-missing areas) could cause a decrease of 0.4 g kg^{-1} in Q_{20m}. This can explain most of the difference in Q_{20m} (0.60 g kg^{-1}) between the two datasets averaged over global oceans. In addition, the successive correction method can induce high values of surface air humidity over the data-sparse regions south of 40°S and contribute additional difference in Q_{20m}. Thus it is believed that the difference of Q_{20m} shown in Fig. 4b most likely due to errors introduced by overestimation of dew point temperatures and the successive correction method of UWM/COADS, although the retrieval may subject to errors.

b. Comparison of wind speed and stress

Figures 6 and 7 compare 1990-93 annual-mean wind speeds, and sea-air humidity and temperature differences between SSM/I and UWM/COADS, with the difference maps shown in Fig. 8. It can be seen from Figs. 6a and 7a that the large-scale patterns of wind speeds are in good agreement between these two datasets. The maxima are located in the strong wind regions of trade winds and extratropical storm tracks. The minima are located in the weak wind areas of ITCZ, SPCZ, and subtropical highs. The retrieved wind speed is generally within ± 1 m s^{-1} of UWM/COADS, but is stronger by ~1-2 m s^{-1} in the northern extratropical oceans (Fig. 8a).

Wentz (1994) estimated a 1.0 m s^{-1} of rms accuracy for his retrieved wind speeds with a 50-km resolution. This high degree of accuracy was estimated by comparing a large number of collocated buoy wind speeds with SSM/I retrievals (with a collocation window of 3 h and 30 km) and by analyzing the retrieval error budget (including spatial-temporal mismatch errors, see Wentz 1997 for the details). On the other hand, da Silva et al. (1994) applied an anemometer height of 20 m to the entire wind dataset measured by ship anemometers to derive a Beaufort equivalent scale for determining visual wind speeds, which depend on sea states. However, Kent and Taylor (1997) found that the true anemometer heights had large standard deviations with the means generally much higher than 20 m and increasing with time. For example, the mean anemometer height was

35.2 m (24.2 m) with a standard deviation of 8.4 m (10.9 m) in midlatitudes of North Pacific (North Atlantic) during 1990. An underestimation of anemometer height can cause high ship anemometer-measured (and visual) wind speeds, as higher wind speeds measured at higher levels are assigned to lower levels. For the same error of anemometer height, the stronger the wind is the larger the wind speed error is. This can cause a larger discrepancy of wind speeds in the high wind regions of the northern extratropical oceans. Table 4 also shows that the biases of wind speed with respect to buoy measurements of the Subduction experiment are smaller for SSM/I than for UWM/COADS, although the differences are not significant. Thus the SSM/I 20-m wind speeds shown in Fig. 6a is believed to be more reliable than that of UWM/COADS shown in Fig. 7a.

The differences of 1990-93 annual-mean wind stresses, LHF, and SHF between SSM/I and UWM/COADS are shown in Fig. 9, with the mean fields compared in Figs. 10 and 11. Figure 9a shows that the retrieved wind stress is generally within $\pm$ 0.02 N m^{-2} of UWM/COADS, except for the southern oceans. Although Figs. 10a and 11a show that the wind stresses follow closely their respective wind fields (Figs. 6a and 7a), Figs. 8a and 9a indicate that the wind directions in the extratropical oceans are steadier for SSM/I than for UWM/COADS. Again, we believe the retrieved wind stress field (Fig. 10a) is more reliable than that of UWM/COADS (Fig. 11a).

c. Comparison of LHF and SHF

The large-scale patterns of LHF (Figs.10b and 11b) are similar between SSM/I and UWM/COADS. The Maximum LHF is found in the Kuroshio Current and Gulf Stream areas, resulting from high winds coupling with large sea-air humidity difference (Q_S-Q_{20m}) during cold air outbreaks in the winters, and the trade wind belts. The minimum LHF is found in the eastern equatorial Pacific and Atlantic, due to up-welling induced cold SSTs associated with weak winds, and the high latitudes due to poleward decrease in SST. However, compared to UWM/COADS, the retrieved LHF is generally larger, but is slightly smaller in the ITCZ and SPCZ (Fig. 9b). The LHF difference in the trade wind zones and the southern oceans is especially large reaching ~40-60 W m^{-2}. This is because SSM/I has significantly larger Qs-Q_{20m} (up to ~ 1-1.5 g kg^{-1}) and slightly

stronger winds in the regions as compared to UWM/COADS (Figs. 8a, 8b, and 9b). Note that, Figs. 4b and 8b show that the difference in Q_{20m} between the two datasets essentially controls that of Q_S-Q_{20m}. This is because the differences in SST and, hence, Q_S between the two datasets are generally negligibly small, except for the southern oceans.

Some climatological studies suggested that the latent heat fluxes based on ship measurements might be systematically underestimated (Oberhuber 1988; da Silva et al. 1994; Josey et al. 1999). Using the COADS original dew point temperatures with revised wind speeds, da Silva et al. (1994) found that the long-term (1945-89) annual-mean net heat flux into the ocean was 30.2 W m^{-2} over the entire ocean. They suggested the surplus of heat flux to be mainly due to the overestimation of solar radiation and the underestimation of latent heat flux. To have the derived meridional oceanic heat transports consistent with the observations meanwhile achieving a global heat balance, they suggested a 7% reduction for the estimated solar radiation but a 15-17% increase for the estimated LHF. Averaged over global oceans, the retrieved LHF is larger than that of UWM/COADS by 23.5 W m^{-2}, which is 27% of the latter. Thus our result generally agrees with their study. Josey et al. (1999) also found an oceanic gain of 30 W m^{-2} for their COADS-based air-sea flux climatology (1980-93). In addition, to achieve global heat balance, Oberhuber (1988) constrained his COADS-derived surface fluxes by reducing 10% of estimated solar radiation and increasing latent heat flux. The latter was achieved by using an enhanced roughness length to increase the transfer coefficient for latent heat flux.

The patterns of SHF (Fig. 10c and 11c) and SST-T_{20m} (Figs. 6c and 7c) are in generally agreement between both datasets. The SHF is generally very small (<10 W m^{-2}) due to the smallness of sea-air temperature difference (<1°C), except for slightly larger fluxes in the northwestern parts of the North Pacific and North Atlantic caused by cold air outbreaks. Figure 8c shows that the discrepancy of SST-T_{20m} between the two datasets is generally very small (~0.2-0.5°C). The retrieved SHF is generally within ±5 W m^{-2} of UWM/COADS, except for some areas

in the extratropics, where the differences in wind speed have large impact on SHF differences (Figs. 8a, 8c and 9c).

8. Concluding remarks

The GSSTF 1.0 dataset has been produced and is available from of the NASA/GSFC DAAC. It has a spatial resolution of 2.0°x2.5° latitude-longitude. It provides daily- and monthly-mean surface turbulent fluxes and some relevant parameters over global oceans for individual F8, F10, and F11 satellites covering the period July 1987-December 1994. It also provides 1988-94 annual- and monthly-mean climatologies of the same variables, using only F8 and F11 satellite data. The retrieved surface air humidity is found to be generally accurate as validated against the collocated radiosonde observations during February and August 1988 and the entire annual cycle of 1993. However, the retrieved surface air humidity (thus LHF) is slightly more accurate for F11 than for F10. In addition, there are significant regional differences of surface air humidity and LHF between the two satellites. This may be due to the orbital drift of the F10 satellite. Thus we only use F8 and F11 results to compute annual- and monthly-mean climatologies in the GSSTF 1.0 dataset. The retrieved daily wind stress and latent heat flux retrieved from the F10 and F11 SSM/Is show useful accuracy as verified against those of the RV Moana Wave and IMET buoy measured in the western Pacific warm pool during the COARE IOP. The1988-94 seasonal-mean wind stress, LHF, wind speed and sea-air humidity difference, derived from monthly climatologies of the GSSTF 1.0 dataset, show reasonable patterns related to seasonal variations of the atmospheric general circulation and are consistent with previous studies.

The patterns of the1990-93 annual-mean turbulent fluxes and input variables are generally in good agreement between SSM/I and UWM/COADS. The retrieved wind speed is generally within ± 1 m s^{-1} of UWM/COADS, but is stronger by ~1-2 m s^{-1} in the northern extratropical oceans. Da Silva et al. (1994) most likely underestimated anemometer heights (Kent and Taylor 1997), which could overestimate wind speeds particularly over high-wind regions of the northern extratropical oceans. The retrieved wind stress is generally within $\pm$ 0.02 N m^{-2} of

UWM/COADS, except for the southern oceans. The results indicate that the wind directions in the extratropical oceans are steadier for SSM/I than for UWM/COADS.

Compared to UWM/COADS, the retrieved LHF and sea-air humidity difference are generally larger with significant differences in the trade wind zones and the southern oceans (up to~40-60 W m^{-2} and ~ 1-1.5 g kg^{-1}). The difference in the surface air humidity between the two datasets is primarily responsible for these discrepancies. The humidity difference is believed to be mainly caused by higher UWM/COADS surface air humidity arising from the overestimation of dew point temperatures and from the extrapolation of observed high humidity southward into data-void regions of the southern oceans. For some stations in the trade wind regions and southern extratropical oceans, the retrieved surface air humidity compares well with the collocated radiosonde observations but its 1990-93 mean values are significantly smaller than those of UWM/COADS. The comparison with the measurements at the SW buoy of the Subduction experiment (Moyer and Weller 1997) also suggests the COADS surface air humidity to be overestimated. This is consistent with some previous findings that ships overestimated dew point temperatures (Isemer and Hasse 1987; Kent et al. 1993; da Silva et al. 1994; Chou et al. 1997; Josey et al. 1999). Averaged over global oceans, the retrieved 1990-93 annual-mean LHF and Q_S-Q_{20m} are larger than UWM/COADS by 23.5 W m^{-2} and 0.55 g kg^{-1}, respectively. This result is consistent with previous studies that the latent heat fluxes based on ship measurements might be systematically underestimated (Oberhuber 1988; da Silva et al. 1994; Chou et al. 1997; Josey et al. 1999). The retrieved SHF is generally within ± 5 W m^{-2} of UWM/COADS, except for some areas in the extratropics, where the differences in wind speed have large impact on SHF differences.

The GSSTF 1.0 dataset derived from SSM/I is useful for climate studies, forcing of ocean models, and validation of coupled ocean-atmosphere global models. Work is on-going to produce a new dataset of daily surface turbulent fluxes, with a 1° x 1° latitude-longitude resolution over global oceans, using the Pathfinder SSM/I 10-m wind speeds and total precipitable water of Wentz (1997) and the SSM/I 10-m wind directions produced by the NASA/GSFC Data Assimilation

Office. This flux dataset is anticipated to have a better accuracy because of improved quality and resolution of the input data.

Acknowledgments This study was supported by the TRMM Program and Physical Oceanography Program, NASA/Office of Earth Science. The SSM/I data of total precipitable water, wind speeds, and antenna temperatures were provided by F. Wentz. The NCEP SSTs were provided by R. W. Reynolds. The sea-air temperature differences were provided by the ECMWF. The flux data of the RV Moana Wave were provided by C. Fairall. The 7.5-min mean turbulent fluxes of IMET buoy were computed by R. A. Weller and S. P. Anderson. The COADS turbulent fluxes were provided by A. da Silva. Consultation related to the computer codes of the Wentz SSM/I antenna temperature was provided by G. J. Huffman. The GSSTF 1.0 dataset was archived at the NASA/GSFC DAAC through the help of L. Chiu and W. Tang.

REFERENCES

Agee, E. M. and R. P. Howley, 1977: Latent and sensible heat flux calculations at the air-sea interface during AMTEX 74. *J. Appl. Meteor., 16,* 443-447.

Atlas, R., R. N. Hoffman, S. C. Bloom, J. C. Jusem, and J. Ardizzone, 1996: A Multiyear Global Surface Wind Velocity Dataset Using SSM/I Wind Observations. *Bull. Amer. Meteor. Soc.*, **77**, 869-882.

Chou, S.-H., 1993: A comparison of airborne eddy correlation and bulk aerodynamic methods for ocean-air turbulent fluxes during cold-air outbreaks. *Bound.-Layer Meteor.*, **64**, 75-100.

Chou, S.-H. and M. P. Ferguson, 1991: Heat Fluxes and Roll Circulations over the Western Gulf Stream During an Intense Cold-Air Outbreak. *Bound.-Layer Meteor.*, **55**, 255-281.

Chou, S.-H., R. M. Atlas, C.-L. Shie and J. Ardizzone, 1995: Estimates of surface humidity and latent heat fluxes over oceans from SSM/I data. *Mon. Wea. Rev.*, **123**, 2405-2425.

Chou, S.-H., C.-L. Shie, R. M. Atlas and J. Ardizzone, 1997: Air-sea fluxes retrieved from Special Sensor Microwave Imager data. *J. Geophys. Res.*, **102**, 12705-12726.

Chou, S.-H., W. Zhao, and M.-D. Chou, 2000: Surface heat budgets and sea surface temperature in the Pacific warm pool during TOGA COARE. *J. Climate,* **13**, 634-649.

Clayson, C. A. and J. A. Curry, 1996: Determination of surface turbulent fluxes for the Tropical Ocean-Global Atmosphere Coupled Ocean-Atmosphere Response Experiment: Comparison of satellite retrievals and in situ measurements. *J. Geophys. Res.,* **101**, 28515-28528.

Curry, J. A., C. A. Clayson, W. B. Rossow, R. Reeder, Y.-C. Zhang, P. J. Webster, G. Liu, R.-S. Sheu, 1999: High-resolution satellite-derived dataset of the surface fluxes of heat, freshwater, and momentum for the TOGA COARE IOP. *Bull. Amer. Meteor. Soc.*, **.80**, 2059-2080.

da Silva, A, C. C. Young and S. Levitus, 1994: Atlas of Surface Marine Data 1994 Vol. 1: Algorithms and Procedures. NOAA Atlas NESDIS 6, US Dept. of Commerce, NOAA, NESDIS, Washington, DC, 83 pp.

Esbensen, S. K., D. B. Chelton, D. Vickers and J. Sun, 1993: An analysis of errors in Special Sensor Microwave Imager evaporation estimates over the global oceans. *J. Geophys. Res., **98** (C4),* 7081-7101.

Fairall, C., E. F. Bradley, D. P. Rogers, J. B. Edson, and G. S. Young, 1996: Bulk parameterization of air-sea fluxes for Tropical Ocean Global Atmosphere Coupled Ocean-Atmosphere Response Experiment. *J. Geophys. Res.*, **101** (C2), 3747-3764.

Hellerman , S. and M. Rosenstein, 1983: Normal monthly wind stress over the world ocean with error estimates. *J. Phys. Oceanogr.*, **13**, 1093-1104.

Isemer, H.-J. and L. Hasse, 1987: The Bunker Atlas of the North Atlantic Ocean. Vol. 2: Air-sea interactions. Springer Verlag, 252 pp.

Josey, S. A., E. C. Kent and P. K. Taylor 1999: New insights into the ocean heat budget closure problem from analysis of the SOC air-sea flux climatology. *J. Climate*, **12**, 2856 - 2880.

Kent, E. C., P. K. Tayor, B. S. Truscott and J. S. Hopkins, 1993: The accuracy of voluntary observing ship's meteorological observations - Results of the VSOP-NA. *J. Atmos. & Oceanic Tech., **10**,* 591-608.

Kent, E. C., and P. K. Taylor, 1997: Choice of a Beaufort equivalent scale. *J. Atmos. Oceanic Technol.*, **14**, 228-242.

Kent, E. C., P. K. Taylor and P. G. Challenor, 2000: The characteristics of a sea surface temperature dataset smoothed by successive correction. *J. Climatel*, **13**, 1845-1857.

Moyer, K. A, and R. A. Weller, 1997: Observations of surface forcing from the Subduction Experiment: A comparison with global model products and climatological datasets. *J. Climate*, **10**, 2725-2742.

Oberhuber, J. M., 1988: *An Atlas Based on the COADS Data Set: The Budgets of Heat, Buoyancy, and Turbulence Kinetic Energy at the Surface of the Global Ocean.* Rep. No. 15, Max-Plank Inst. for Meteorol., Hamburg, Germany.

Reynolds, R. W. and T. S. Smith, 1994: Improved global sea surface temperature analyses. *J. Climate.*, **7**, 929-948.

Schluessel, P., L. Schanz, and G. Englisch, 1995: Retrieval of latent heat flux and longwave irradiance at the sea surface from SSM/I and AVHRR measurements. *Adv. Space Res.*, **16**, 107-116.

Schulz, J., P. Schluessel and H. Grassl, 1993: Water vapor in the atmospheric boundary layer over oceans from SSM/I measurements. *Int. J. Rem. Sens.*, **14**, 2773-2789.

Schulz, J., J. Meywerk, S. Ewald, and P. Schluessel, 1997: Evaluation of satellite-derived latent heat fluxes. *J. Climate*, **10**, 2782-2795.

Schulz, J. and V. Jost, 2000: A New Satellite-Derived Freshwater Flux Climatology: The Hamburg Ocean Atmosphere Parameters and Fluxes from Satellite Data. *J. Climate*, (submitted).

Webster, P., C. A. Clayson, and J. A. Curry, 1996: Clouds, radiation, and the diurnal cycle of sea surface temperature in the tropical western Pacific. *J. Climate*, **9**, 1712-1730.

Weller R. A. and S. P. Anderson, 1996: Surface meteorology and air-sea fluxes in the western equatorial Pacific warm pool during the TOGA Coupled Ocean-Atmosphere Response Experiment. *J. Climate,* **9**, 1959-1990.

Wentz, F. J., 1993: User's Manual SSM/I Antenna Temperature Tapes. Revision 2. Tech. Rep. 060989, 16 pp. [Available from Remote Sensing Systems, Santa Rosa, CA 95404.]

Wentz, F. J., 1994: User's Manual SSM/I-2 Geophysical Tapes. Tech. Rep. 070194, 20 pp. [Available from Remote Sensing Systems, Santa Rosa, CA 95404.]

Wentz, F. J., 1997: A well calibrated ocean algorithm for SSM/I. *J. Geophys. Res.*, **102**, 8703-8718.

Wick, G. A., W. J. Emery and L. H. Kantha, 1996: The behavior of the bulk-skin sea surface temperature difference under varying wind speed and heat flux. *J. Phys. Oceanogr.* **26**, 1969-1988.

Woodruff, S. D., R. J. Slutz, R. L., Jenne and P. M. Steurer, 1987: A comprehensive ocean-atmosphere data set. *Bull. Amer. Meteor. Soc.*, **68**, 1239-1250.

Woodruff, S. D.,S. J. Lubker, K. Wolter, S. J. Worley, and J. D. Elm, 1993: Comprehensive Ocean-Atmosphere Data Set (COADS) release 1a: 1980-92. *Earth Syst. Monit.*, **4**, 4-8.

Table 1. Radiosonde stations for collocation validation.

Name	Number	Latitude	Longitude
	Indian Ocean		
Port Blair	43333	11.67°N	92.72°E
Minicoy Island	43369	8.30°N	73.00°E
Seychelles	63985	4.67°S	55.52°E
Diego Garcia	61967	7.35°S	72.48°E
Cocos Island	96996	12.18°S	96.83°E
I. N. Amsterdam	61996	37.80°S	77.53°E
	Pacific Ocean		
St. Paul Island	70308	57.15°N	170.22°W
Nikolskoye-on-Bering	32618	55.20°N	165.98°E
Hachijajima	47678	33.12°N	139.78°E
Minamidaito	47945	25.83°N	131.23°E
Ishigakijima	47918	24.33°N	124.17°E
Isla Guadalupe	76151	29.17°N	118.32°W
Isla Socorro	76723	18.72°N	110.95°W
Wake Island	91245	19.28°N	166.65°E
Guam	91217	13.55°N	144.83°E
Willis Island	94299	16.30°S	149.98°E
Pago Pago	91765	14.33°S	170.72°W
Tahiti Island Faaa	91938	17.55°S	149.62°W
Easter	85469	27.17°S	109.43°W
Lord Howe Island	94995	31.53°S	159.08°E
Campbell Island	93944	52.55°S	169.15°E
Macquarie Island	94998	54.50°S	158.95°E
	Atlantic Ocean		
Mike	C7M	66.00°N	2.00°E
Lima	C7L	57.00°N	20.00°W
Sable Island	71600	43.93°N	60.02°W
Bermuda NAS/Kindley	78016	32.37°N	64.68°W
Roberts Field	78384	19.30°N	81.37°W
San Maarten	78866	18.05°N	63.12°W
Barbados	78954	13.07°N	59.50°W
Isla San Andreas	80001	12.58°N	81.70°W

Table 2. Comparison of retrieved surface air specific humidity with those of radiosonde observations within 100 km and 1.5 h over global oceans and various regions. In the table mean denotes retrieved mean humidity for N collocated data pairs during the periods indicated, positive bias indicates larger retrieved values, and rms denotes the root-mean-square difference. Units are g kg^{-1}.

Satellite	Period	N	Mean	Bias	Rms	Correlation
F8	Feb/88, Aug/88	342	11.61	0.03	1.57	0.97
F10	Feb/93, Aug/93	288	8.95	0.00	1.78	0.94
F11	Feb/93, Aug/93	174	11.35	0.10	1.55	0.97
F10	1993	1205	8.73	0.14	1.96	0.93
F11	1993	849	11.96	0.25	1.62	0.97
F10	1993 (Caribbean)	50	17.34	-0.72	1.83	0.67
F11	1993 (Caribbean)	199	17.55	-0.15	1.69	0.74
F10	1993 (52.5°S, 169°E)	167	5.55	-0.81	1.48	0.56
F11	1993 (52.5°S, 169°E)	12	5.85	-0.07	1.10	0.65
F10	1993 (54.5°S, 159°E)	219	4.73	-0.60	1.30	0.47
F11	1993 (54.5°S, 159°E)	62	4.99	-0.11	1.15	0.55
F11	1993 (Indian Ocean)	499	14.74	0.32	1.80	0.93
F11	1993 (Trop. Indian)	350	17.42	0.51	1.60	0.71
F11	1993(38°S, 77.5°E)	149	8.44	-0.13	2.25	0.57

Table 3. Comparison of daily wind stresses, latent heat fluxes (LHF), and sensible heat fluxes (SHF) derived from the F10 and F11 SSM/Is with those measured at the RV Moana Wave (MW) and IMET buoy during COARE IOP. In the table mean denotes retrieved fluxes averaged over 52 (120) days for the MW (IMET), positive bias indicates larger retrieved fluxes, and rms denotes the root-mean-square difference. Units are W m^{-2} for heat fluxes and 10^{-4} N m^{-2} for wind stress.

Data source	Number of days	Flux	Mean	Bias	Rms		Correlation
					Daily	Monthly	
MW	52	stress	417	61	187	69	0.86
IMET	120	stress	371	-18	211	42	0.78
MW	52	LHF	110.7	6.2	29.0	8.1	0.83
IMET	120	LHF	104.8	-2.4	29.2	5.8	0.71
MW	52	SHF	5.8	0.8	3.8	1.0	0.39
IMET	120	SHF	6.3	-2.6	6.6	2.8	0.40

Table 4. Differences of monthly mean 20-m specific humidity (Q_{20m}) and 20-m wind speed (U_{20m}) derived from WHOI buoys observed during Subduction Experiment, SSM/I (F8 and F11), and UWM/COADS for N months of buoy deployments. Units are g kg^{-1} for Q_{20m} and m s^{-1} for U_{20m},.

Locations	NE buoy (33N, 22W)	NW buoy (33N, 34W)	SE buoy (18N, 22W)	SW buoy (18N, 34W)	CE buoy (26N, 29W)	All buoy
Months	25	12	15	14	20	86
Q_{20m} (SSM/I-buoy)	0.5	0.6	-0.1	0.5	0.4	0.4
Q_{20m} (UWM-buoy)	0.5	0.4	0.3	1.2	0.4	0.6
U_{20m} (SSM/I-buoy)	1.1	1.7	-0.5	0.9	1.0	0.9
U_{20m} (UWM-buoy)	1.3	1.9	1.0	1.2	0.9	1.2

FIGURE CAPTIONS

Fig.1. F10-F11 differences of SSM/I-derived (a)10-m wind speed, (b) 10-m specific humidity, and (c) latent heat flux for 1992-94.

Fig. 2. Seasonal-mean wind stresses for (a) winter, (b) spring, (c) summer, and (d) fall, derived from F8 and F11 SSM/I data during 1988-94. Arrows indicate wind stress directions.

Fig. 3. Same as Fig. 2, except for latent heat fluxes.

Fig. 4. SSM/I-minus-UWM/COADS differences of (a) SST, (b) 20-m specific humidity, and (c) 20-m temperature for 1990-93.

Fig. 5. Monthly-mean 20-m specific humidity derived from measurements at NE buoy of the Subduction Experiment (solid line), and SSM/I (solid circles) and UWM/COADS (crosses) of the nearest grid point. Unit: g kg^{-1}.

Fig. 6. Annual-mean (1990-93) (a) 20-m wind speed, and (b) sea-20m humidity difference, derived from F8 and F11 SSM/I data, and (c) sea-20m temperature difference of ECMWF.

Fig. 7. Same as Fig. 6, except for UWM/COADS.

Fig. 8. SSM/I-minus-UWM/COADS differences of (a) wind speed, (b) sea-air humidity difference, and (c) sea-air temperature difference at the 20-m level for 1990-93.

Fig. 9. SSM/I-minus-UWM/COADS differences of (a) wind stress, (b) latent heat flux, and (c) sensible heat flux for 1990-93. Arrows indicate wind stress difference directions.

Fig. 10. Annual-mean (a) wind stress, (b) latent heat flux, and (c) sensible heat flux, derived from F8 and F11 SSM/I data during 1990-93. Arrows indicate wind stress directions.

Fig. 11. Same as Fig. 10, except for UWM/COADS.

1992–94 F10–F11 Difference

(a) 10m wind speed diff (m/s)

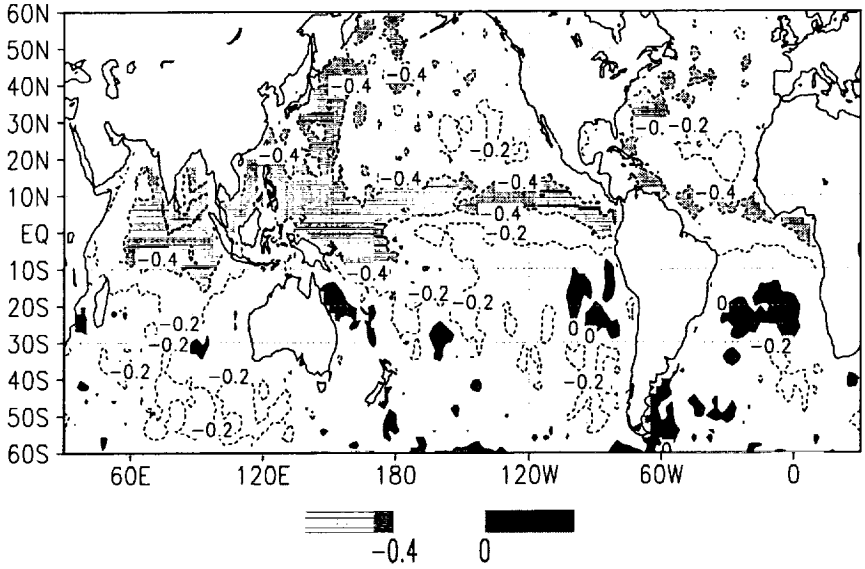

(b) 10m humidity diff (g/kg)

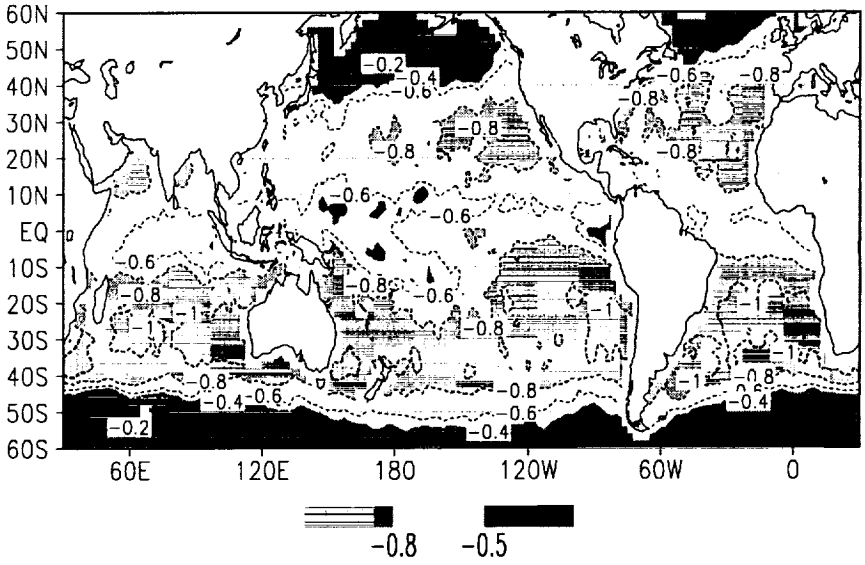

(c) LHF diff (W/m**2)

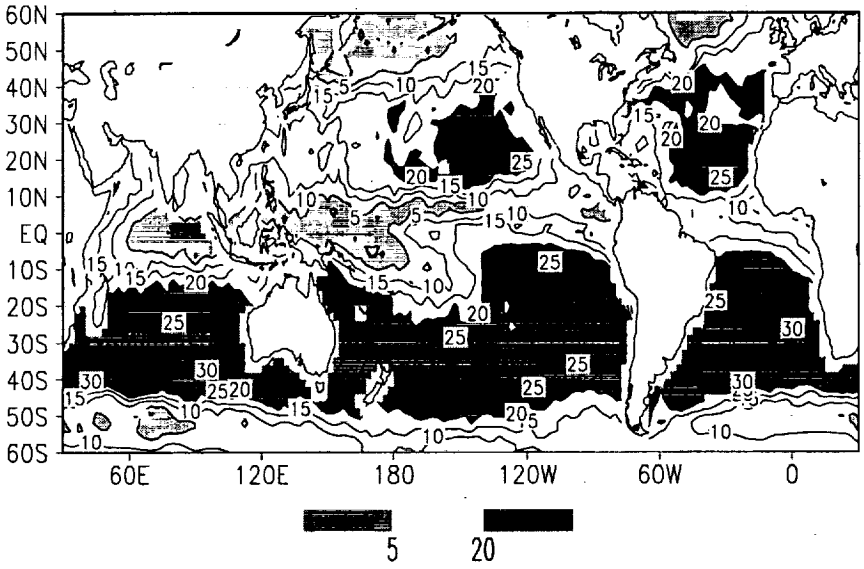

Seasonal Mean SSMI Wind Stress (0.1 N/m**2)

(a) DJF(1988–94)

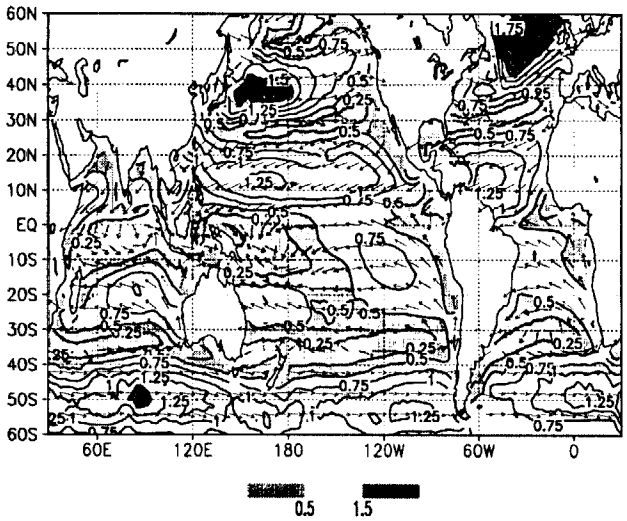

(b) MAM(1988–94) F8 & F11

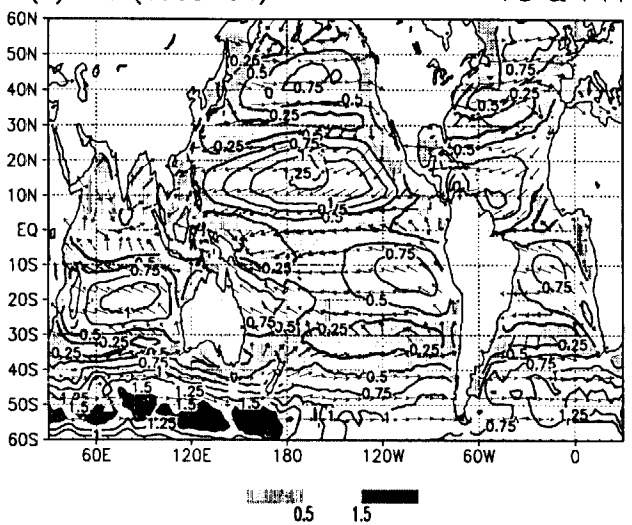

(c) JJA(1988–94)

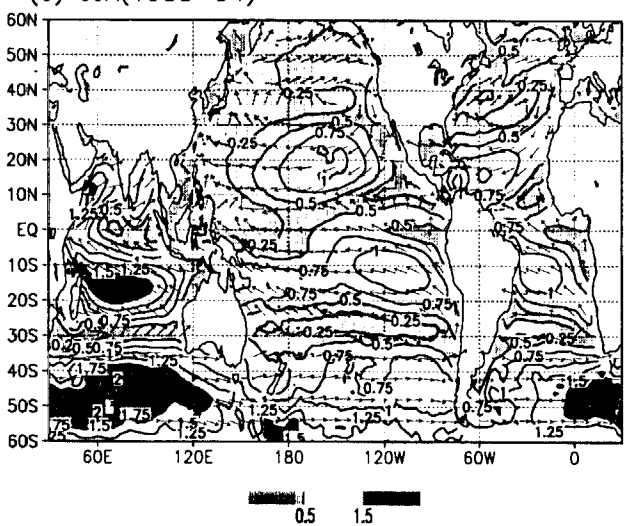

(d) SON(1988–94)

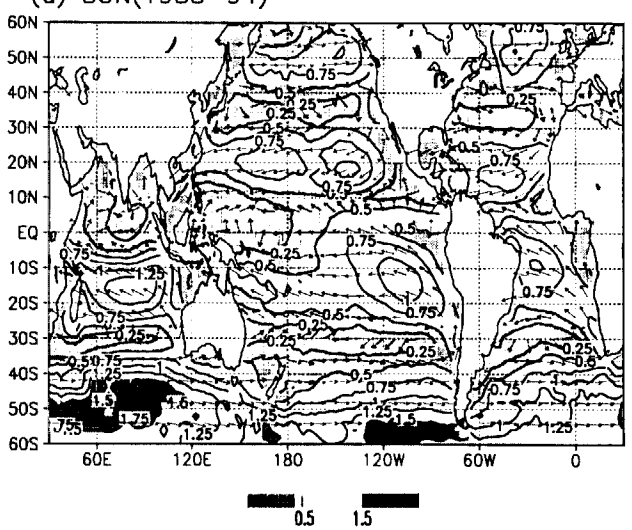

Seasonal Mean SSMI Latent Heat Flux (W/m**2)

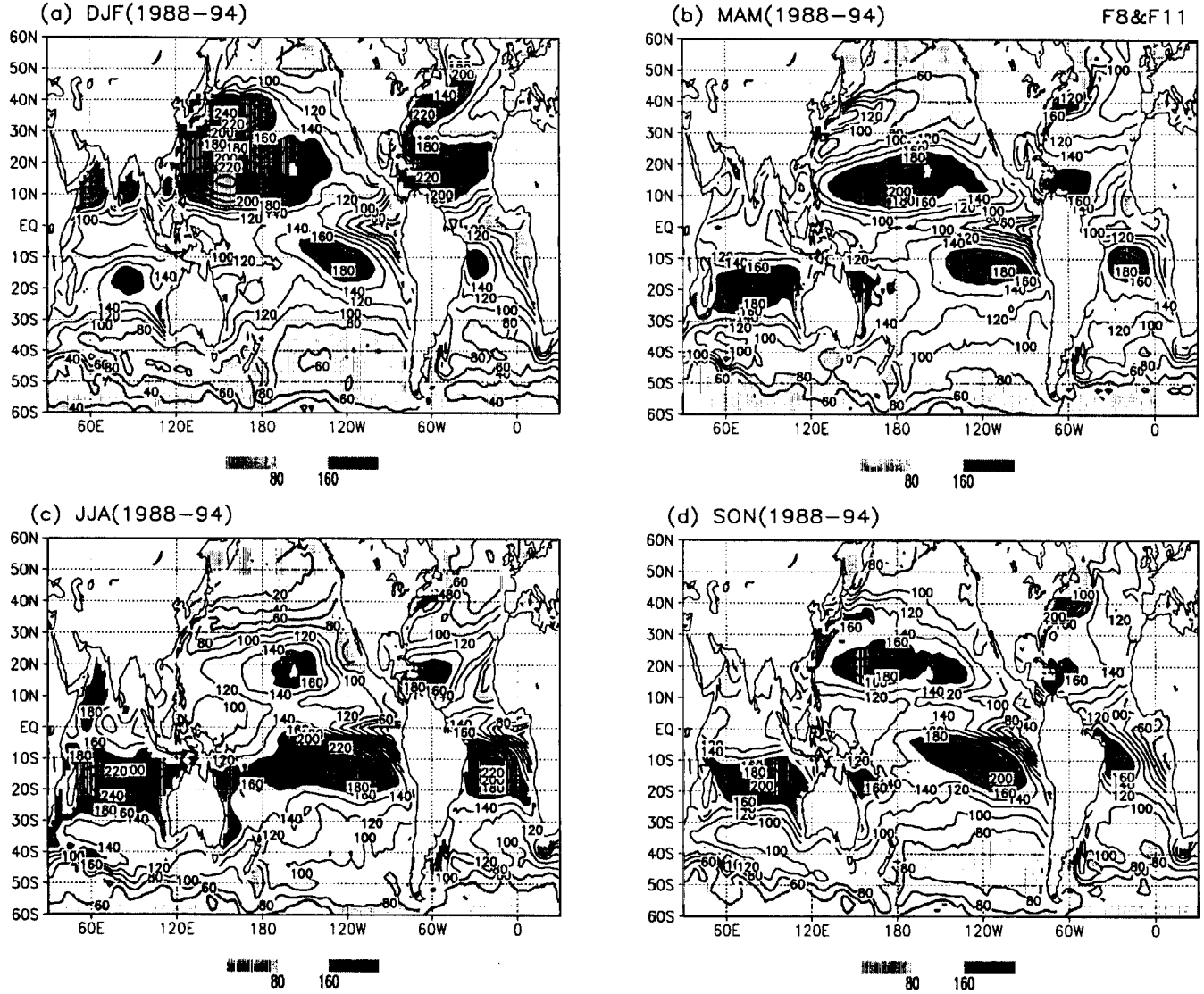

1990–93 Annual Mean SSMI–UWM/COADS Difference

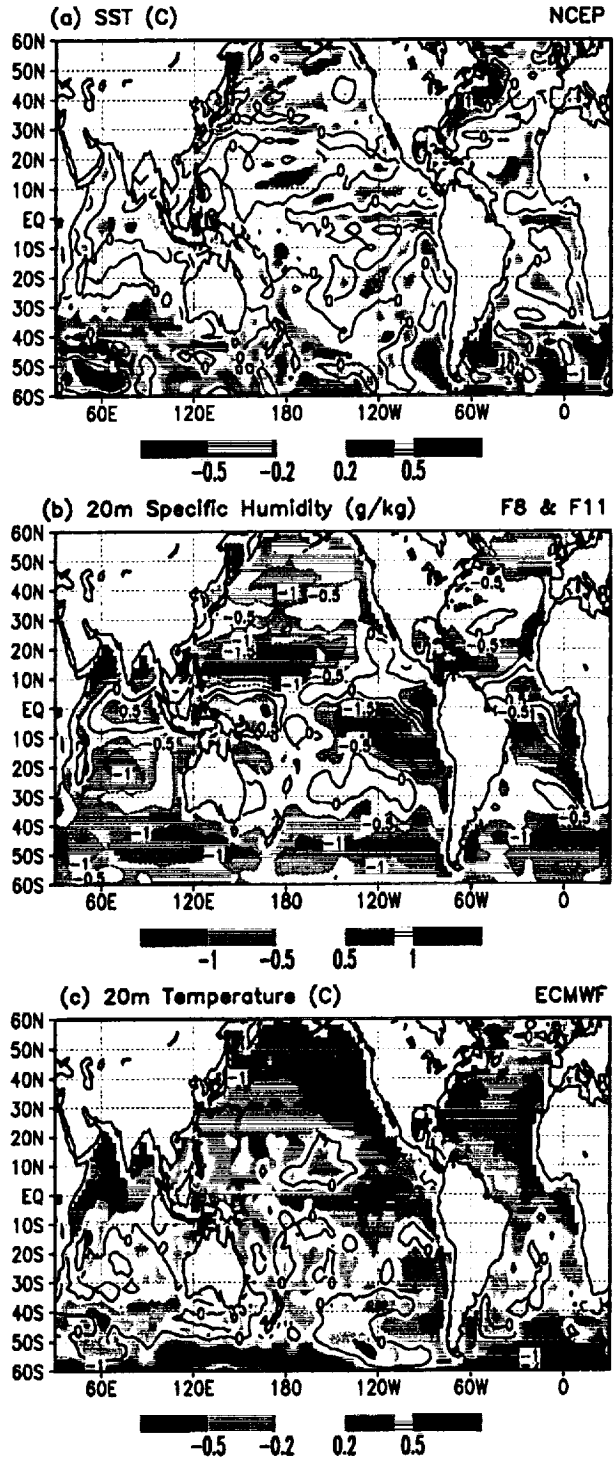

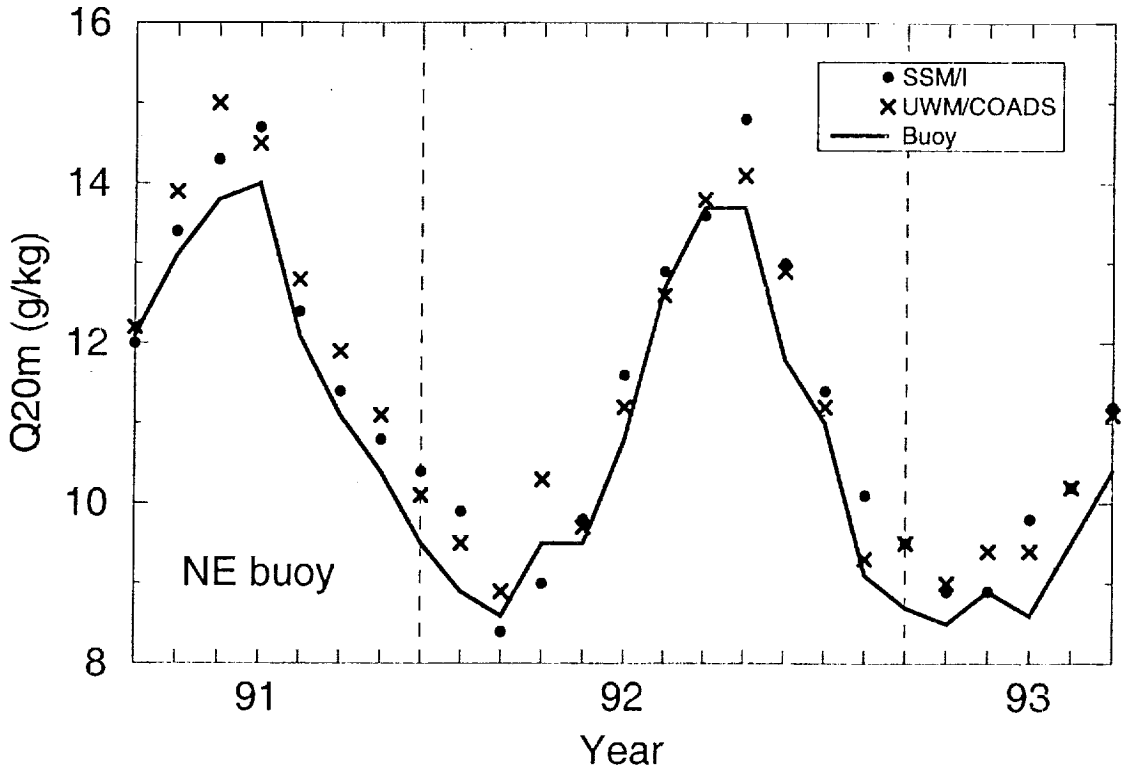
16
14
12
10
8
Q20m (g/kg)
91
92
93
Year
SSM/I
UWM/COADS
Buoy
NE buoy

1990–93 Annual Mean SSMI Parameters

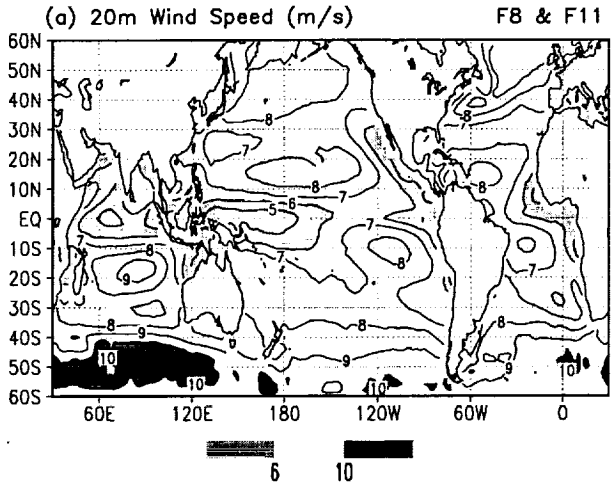

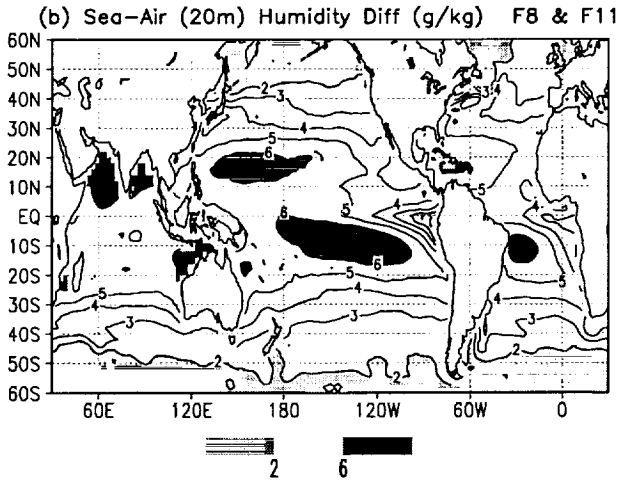

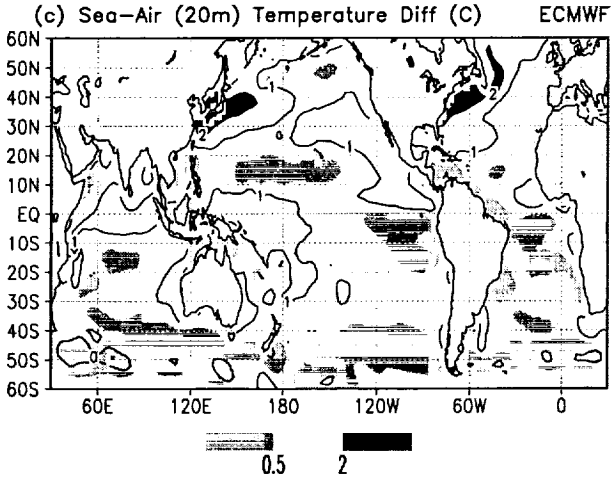

1990–93 Annual Mean UWM/COADS Parameters

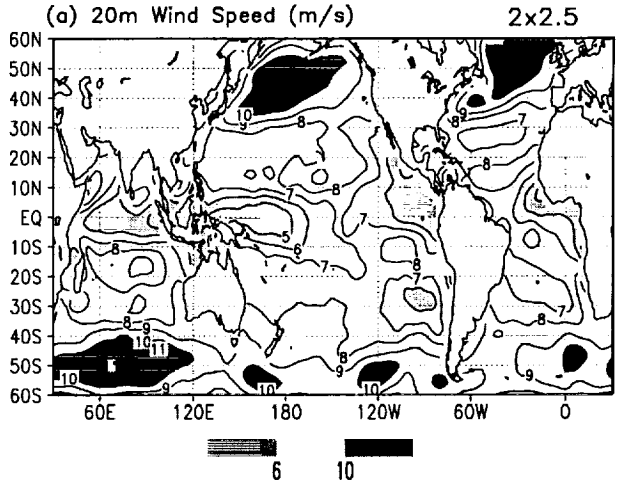

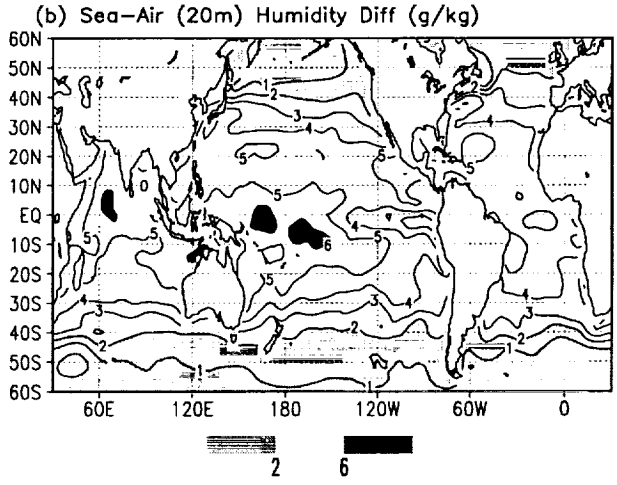

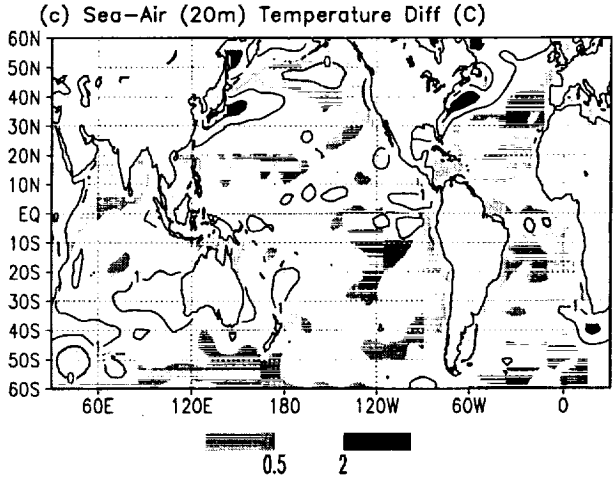

90–93 Annual Mean SSMI–UWM/COADS Diff

(a) 20m Wind Speed (m/s) F8 & F11

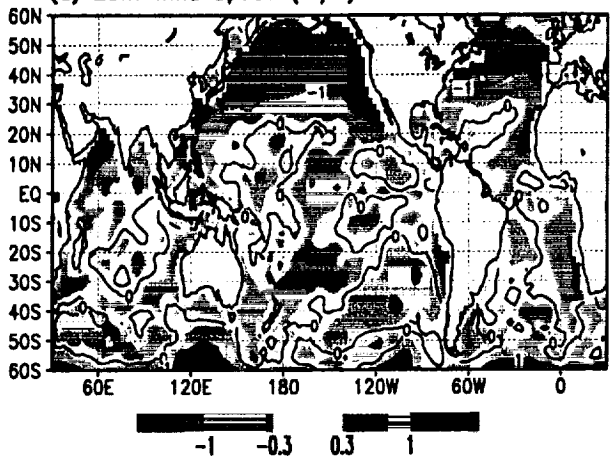

(b) Sea–Air (20m) Humidity Diff (g/kg) F8 & F11

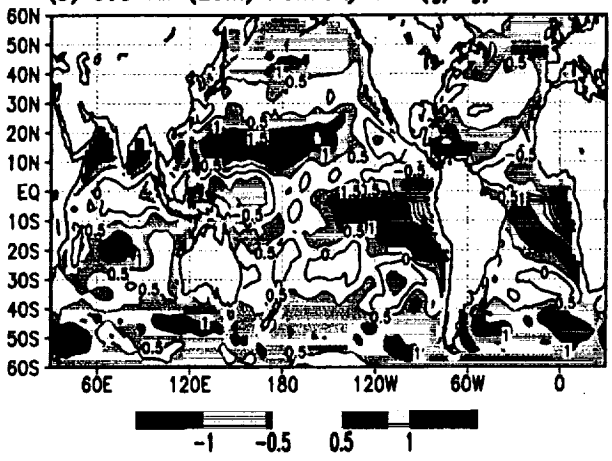

(c) Sea–Air (20m) Temperature Diff (C) ECMWF

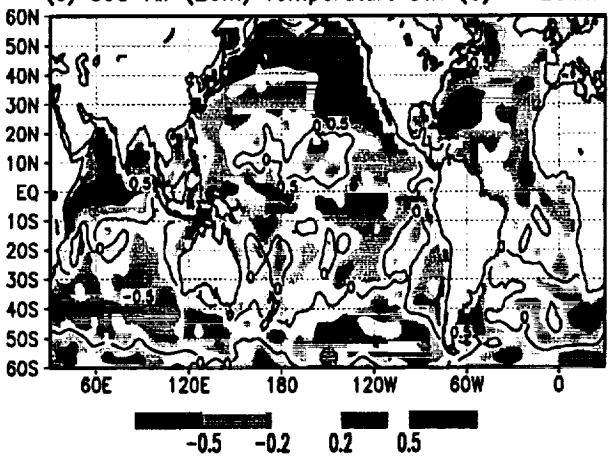

90–93 Annual Mean SSMI–UWM/COADS Diff

(a) Wind Stress (0.1N/m**2) F8 & F11

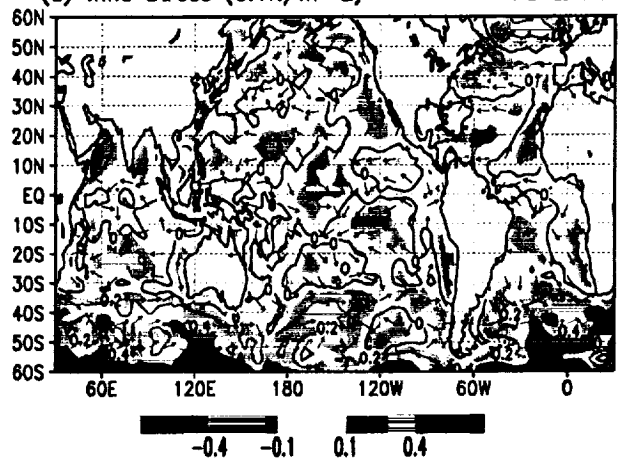

(b) Latent Heat Flux (W/m**2)

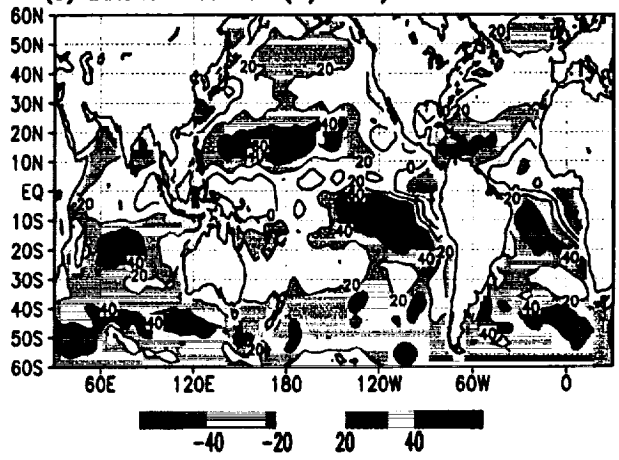

(c) Sensible Heat Flux (W/m**2)

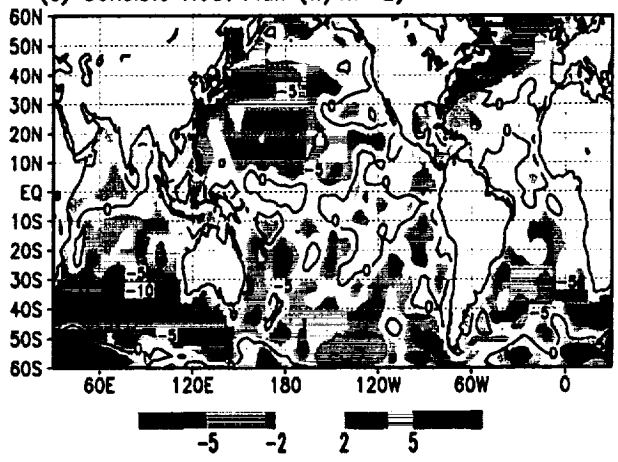

1990–93 Annual Mean SSMI Fluxes

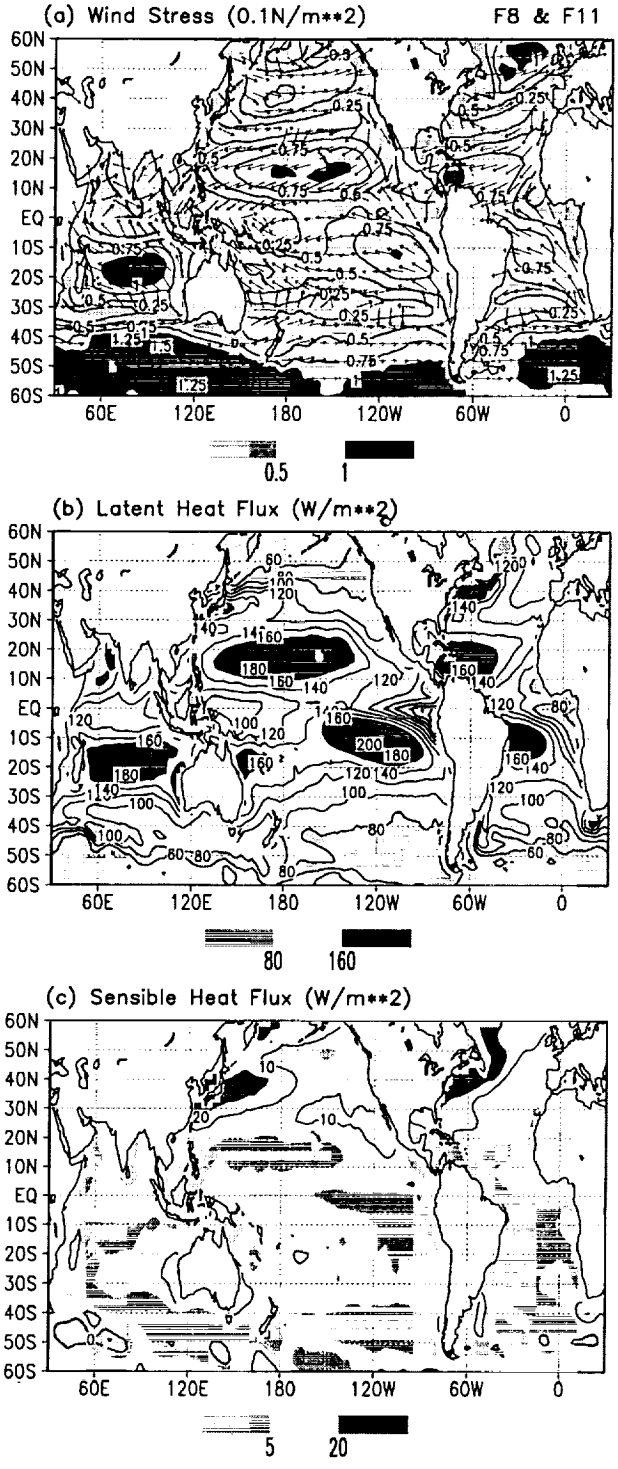

1990–93 Annual Mean UWM/COADS Fluxes